The Relation Between Visibility and the Size-Number Distribution of Airborne Soil Particles

E. M. PATTERSON, D. A. GILLETTE AND G. W. GRAMS

National Center for Atmospheric Research,[1] Boulder, Colo. 80303

(Manuscript received 3 March 1975, in revised form 26 February 1976)

ABSTRACT

Simultaneous visibility observations and size-number distribution measurements of airborne soil particles were made during incidents of soil erosion in west Texas. Visibilities were calculated by applying Mie scattering theory to measured size distributions and were compared with observed visibilities. Agreement was found, and similar comparison with artifical modifications to the observed size distributions demonstrated that any major changes in the observed size distributions would result in significant discrepancies between the observed and the calculated visibilities. These comparisons confirm that under our experimental conditions the optically important particles are those in the size range $0.62<r<20$ μm. The sensitivity of the calculated visibility to modifications in the measured size distribution implies that such comparisons between calculated and observed visibility provide a means of confirming size distribution measurements under a variety of conditions.

1. Introduction

The extinction coefficient for atmospheric particulate matter is related by Mie theory to the size distribution and optical properties of the particles, so simultaneous measurements of size distributions and extinction coefficients provide a means of comparing the two. Ensor *et al.* (1972) calculated the scattering expected from measured size distributions of Los Angeles smog aerosols and compared these predictions to integrating-nephelometer measurements of scattered light; they found agreement within the combined uncertainties of each measurement process. Zuev *et al.* (1965) compared measured extinction coefficients with those calculated from known size distributions of fog droplets and reported good agreement. Since visibility is determined by the total extinction in the atmosphere (Koschmieder, 1924), visibility observations can provide an estimate of the atmospheric extinction coefficient while avoiding problems associated with instrumental measurements of extinction coefficients; simultaneous observations of visibility and measurement of the particle size distribution therefore provide a means of confirming an observed size distribution.

During incidents of soil erosion by wind, we have conducted a series of simultaneous visibility and particle size-distribution measurements, in part to provide a check of our particle-sizing procedures, and in part to determine what quantitative size-distribution measurements are sufficient to predict visibility measurements. We also compared observed visibilities with the visibilities calculated using several artificially modified size distributions designed to test possible uncertainties in particle-sizing techniques that have been suggested by other workers in this field. In addition, we investigated the effect on the calculated visibility of varying the assumed optical properties of the airborne dust.

2. Relation of visual range and particle extinction

Visibility is defined as the greatest distance in a given direction at which a prominent dark object can be seen against the horizon with the unaided eye; the prevailing visibility is defined as the greatest horizontal visibility which is equalled or surpassed through half (not necessarily a continuous half) of the horizon circle (Huschke, 1959). The concept of visibility is made more quantitative by defining a visual range V as the distance from an observer at which the contrast ratio between a black object and a bright background is equal to 0.02. This contrast ratio of 0.02 is taken as the minimum contrast ratio that can be distinguished by the unaided human eye, and this defined visual range will be taken as the measure of the visibility.

The visual range is related to the atmospheric extinction coefficient σ by (Johnson, 1954)

$$V=\frac{|\ln 0.02|}{\sigma}, \tag{1}$$

which becomes

$$V=\frac{3.912}{\sigma}, \tag{2}$$

where σ is composed of two parts—one due to extinction by the air molecules, σ_A, and the other due to extinction

[1] The National Center for Atmospheric Research is sponsored by the National Science Foundation.

by atmospheric particles, σ_P; but for visibilities of less than a few kilometers, $\sigma_P \gg \sigma_A$ and the extinction is completely determined by σ_P, so $\sigma = \sigma_P$. In general, it is assumed that the distribution of atmospheric particles is uniform, leading to uniform σ_P. Under this assumption, measurement or calculation of σ_P at a point should lead to a calculated "point visibility" that is equal to the observed visual range. A general discussion of the problems and limitations of visibility measurements is given in Johnson (1954).

The extinction coefficient may be calculated from Mie theory, which describes scattering by spherical particles. Although our particles are not perfect spheres, electron microscope pictures indicate that they are compact, amorphous solids and the usual assumption is that Mie theory approximately describes the scattering. A complete discussion of applications of the Mie solution of general scattering theory may be found in Deirmendjian (1969), Kerker (1969), or van de Hulst (1957). Assuming that the aerosol particles are uniform homogeneous spheres, we can use the formalism of Mie scattering. The particle extinction cross section is commonly written in terms of the cross-sectional area πr^2 of the particle times an efficiency factor for extinction, Q_{EXT}. Thus,

$$\sigma_P = \pi r^2 Q_{EXT} \tag{3}$$

for a single particle. The extinction efficiency factor, expressed in terms of the Mie amplitude functions a_n and b_n, is

$$Q_{EXT}(m,x) = \frac{2}{x^2} \sum_{n=1}^{\infty} (2n+1)\, \mathrm{Re}(a_n + b_n), \tag{4}$$

where $m = n_{Re} - n_{Im} i$ is the complex index of refraction of an aerosol particle and $x = 2\pi r/\lambda$ is a size parameter relating the radius r of the sphere to the wavelength λ of the incident electromagnetic wave. In this same way, the efficiency factor for scattering is

$$Q_{SCA}(m,x) = \frac{2}{x^2} \sum_{n=1}^{\infty} (2n+1)\{|a_n|^2 + |b_n|^2\}. \tag{5}$$

For a monodisperse aerosol having N_P particles per unit volume, the total σ_P per unit path length is given by

$$\sigma_P = \pi r^2 Q_{EXT} N_P. \tag{6}$$

Similarly, the total extinction due to a polydisperse distribution of particles is given by the integral over the size distribution

$$\sigma_P = \int_{r_1}^{r_2} \pi r^2 Q_{EXT} n(r) dr, \tag{7}$$

where $n(r)$ is a continuous function defined within the radius interval from r_1 to r_2 representing the concentration of particles per unit volume and per unit increment of dr.

Although optical constants for the observations reported in this study have not been measured, particles for similar west Texas dust storm events had $n_{Re} = 1.525$ and $n_{Im} = 0.005$ (Grams *et al.*, 1974). These values are assumed to be representative of the airborne particles associated with our observations and, unless otherwise noted, they are used in our calculations.

Parts (a) and (b) of Fig. 1 show values of Q_{EXT} and Q_{SCA}, respectively, for Mie scatterers with $n_{Re} = 1.525$ and with six different n_{Im} values (0, 0.005, 0.01, 0.02, 0.05, 0.1). In Fig. 1(a), the curves tend to oscillate about a smooth curve that approaches $Q_{EXT} = 2$ for large particles; the largest oscillations about this curve are those associated with non-absorbing particles ($n_{Im} = 0$), and the amplitude of these oscillations decreases as the value of n_{Im} increases. In Fig. 1(b), $Q_{SCA} = Q_{EXT}$ for non-absorbing particles but, as n_{Im} increases, the Q_{SCA} values decrease, approaching the value $Q_{SCA} = 1$ for large particles. The efficiency factor for total extinction is the correct value to use in visibility calculations since

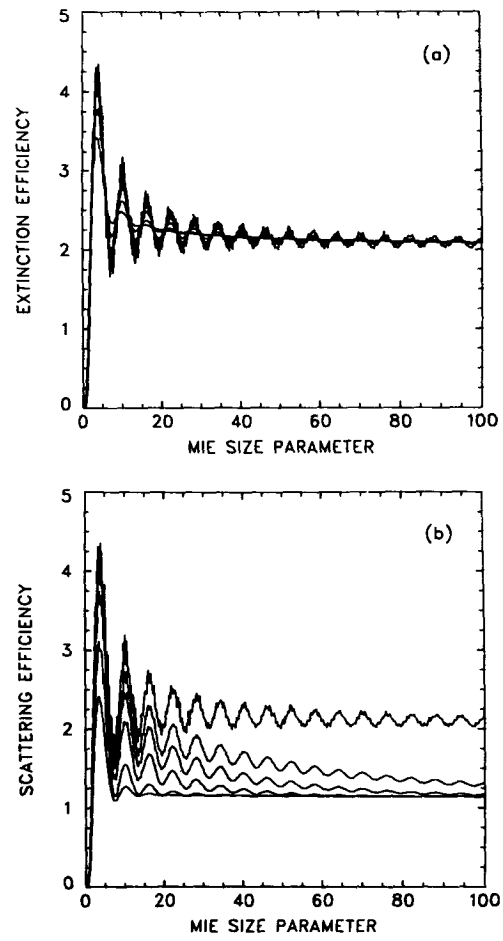

FIG. 1. Extinction efficiency (a) and scattering efficiency (b) for Mie scatterers with $n_{Re} = 1.525$ and $n_{Im} = 0.0$, 0.005, 0.01, 0.02, 0.05 and 0.10 plotted against the Mie size parameter $x = 2\pi r/\lambda$. See text for details.

only unscattered light reaches the observer; further discussion of this point may be found in Kerker (1969). As a final note, we point out that since only minor changes in Q_{EXT} are associated with changes in n_{Im}, our visibility calculations will not be appreciably affected by our choice of n_{Im}.

3. Field observations

Our field observations were conducted in Texas in March and April of 1973 and 1974, during periods of moderate-to-severe wind erosion (soil movement greater than 0.01 g s^{-1} cm^{-1}). We specify conditions of "blowing dust" to correlate with $V<11$ km, "dust storm" to correlate with $V<1$ km, and "severe dust storm" to correlate with $V<0.5$ km, as defined in the Federal Meteorological Handbook No. 1 (U. S. Dept. of Commerce *et al.*, 1970). Observations were made on sites approximately 1.6 km square. Our data consisted of visibility observations and particle size-distribution determinations taken simultaneously. Particle size distributions were used to calculate visibilities for comparison with the observed visibilities.

Observations of the visual range were made at a height of approximately 2 m, using reference objects against the horizon. Where possible, equally spaced telephone poles were used as references, and the visibility was determined by counting the number of telephone poles that could be seen. Where telephone poles were not suitably placed, other dark references at known distances from the observers were used. The particulate loading in the atmosphere was not steady because of the gusty wind, a situation leading to time variations in visibility. The effect of such conditions is to increase the uncertainty in the determination of each data point and thus to increase the scatter in the data when calculated visibilities are plotted against observed visibilities.

4. Particle size distributions

Particle size distributions at a height of 2 m (the height at which visibility observations were made) were determined for particles with radii $0.62<r<250$ μm. Two different methods were used for different portions of the size range. For the smaller particles, the collection and sizing methods described by Gillette *et al.* (1972) were used. Airborne particles were collected using a membrane filter device consisting of a removable filter cassette mounted in a wind vane, as shown in Fig. 2. Air was drawn through the device at a rate of 12.5 liters min^{-1} (using an isokinetic nozzle facing into the wind). Interchangeable nozzles allowed isokinetic sampling under varying wind conditions and the sampling-time interval was adjusted to obtain particle numbers suitable for counting.

Two such devices were used to obtain particle size

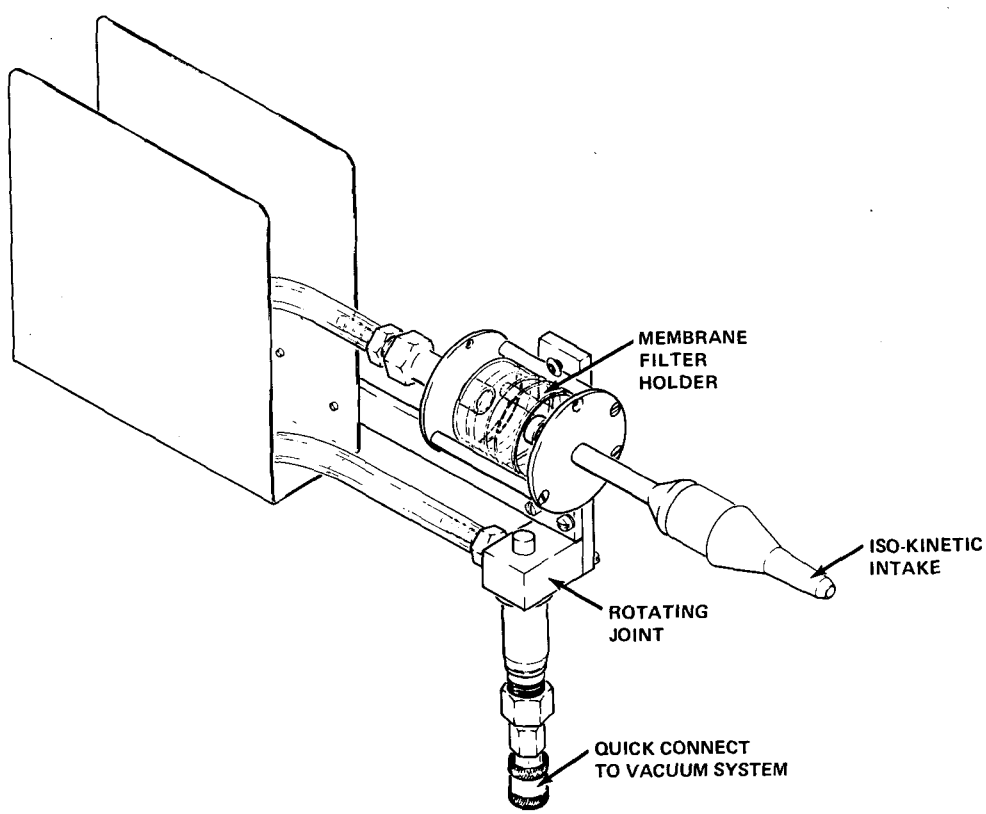

FIG. 2. The mechanical arrangement of the filter and filter-holder assembly.

distributions at two heights (1.5 and 6 m for the 1973 samples, and 1.0 and 6.8 m for the 1974 samples). The particle size distribution at 2 m was inferred by logarithmic interpolation from the measured distributions above and below 2 m, using the form of the height variation in concentration of dust measured by Chepil and Woodruff (1957).

The exposed filters were prepared for microscopic examination as described by Gillette *et al.* (1972). Particle sizes were analyzed by the automated image-scanning system described by Blifford and Gillette (1973), with several magnifications used to give statistical accuracy in the particle size range selected. Particle size intervals (μm) were chosen to be logarithmically equal (0.62–1.24, 1.24–2.48, 2.48–4.96, 4.96–9.89 and 9.89–19.73).

We also analyzed several samples with an alternate method which is more adapted to submicron particle size ranges. Particles smaller than 1 μm in radius were counted from scanning electron microscope photographs of the surfaces of Nuclepore filters having pores 0.2 μm in radius; the filter was scanned radially, and magnifications of up to 10 000 times were used. The counting was carried out using a Zeiss TGZ-3 semi-automatic particle counter to size each particle into one of 48 equal logarithmic size intervals. These size intervals were then combined into 12 intervals which varied from 0.1 to 1 μm in radius. The Nuclepore filters are 100% efficient for particles larger than $r=0.2$ μm since they act as a sieve for those particles; in addition, their efficiency is greater than 50% for particles as small as $r=0.1$ μm. Nuclepore filter efficiencies have been determined by Spurny *et al.* (1969), and the size distribution of submicron particles was determined with the aid of their results.

In general, the electron microscope examinations confirmed the size distribution results obtained with our automated image-scanning apparatus, showing that—under our experimental conditions—the relative concentration of particles with $r<0.62$ μm was so small that their optical effects would be negligible. We felt, then, that an unjustifiable amount of effort would be required to apply standard manual sizing procedures to extend the size distribution analysis to the resolution limit of our optical microscope (0.3 μm radius) or to apply electron microscope analysis for particles with $r<0.3$ μm. We therefore let the lower limit of the particle sizing analysis coincide with that of our automated image-scanning system (0.62 μm).

The upper size limit of this technique for determing the particle size distribution is constrained by the small number of counts for particles with radii >10 μm. Since sampling times were necessarily short and the relatively larger particles were less numerous than particles in the size range $1<r<10$ μm, fewer of the larger particles were counted (typically, five particles in the size range 9.89–19.73 μm were obtained during the sampling interval). The counting uncertainties (the square root of the number of counts for a Poisson distribution) are therefore on the order of 50% of the counts observed in this range; for larger radii (with even smaller counts) the uncertainties increase, so the results at larger sizes have decreasing significance. Although we show that these larger particles contribute little to the total light scattered, we felt that a reasonably accurate knowledge of the total number present was needed to correctly assess the scattering contributions of these particles. More accurate size-distribution measurements for these larger particles were obtained by analysis of samples collected with an NCAR-modified Bagnold catcher.

As described by Gillette and Goodwin (1974) and shown in Fig. 3, the Bagnold instrument collects par-

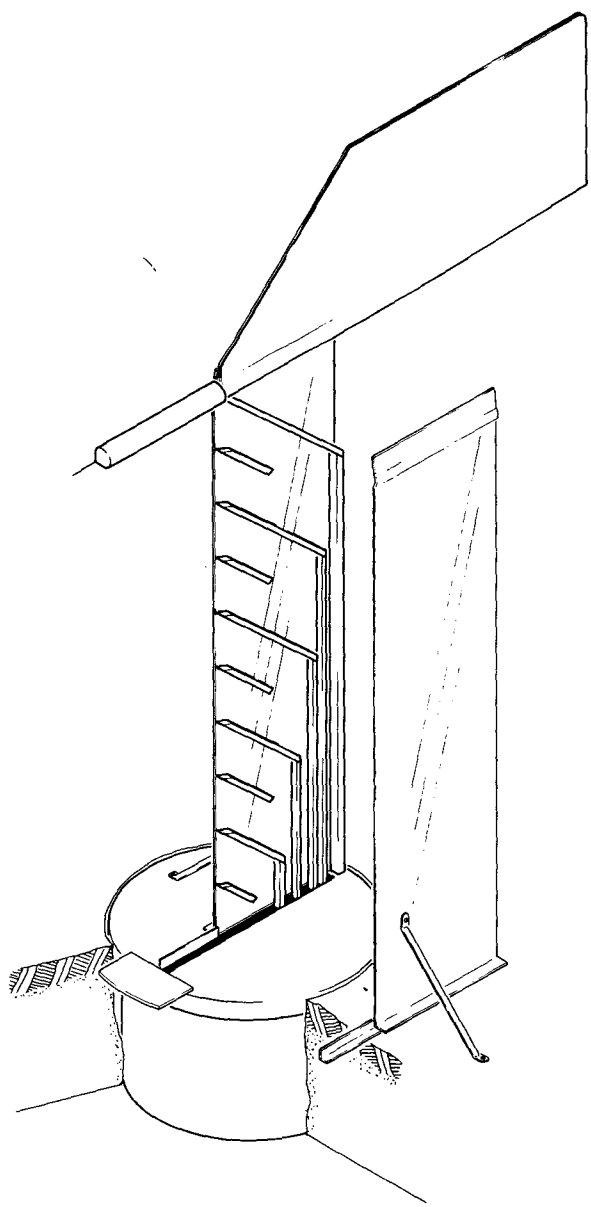

FIG. 3. Cutaway view of NCAR-modified Bagnold catcher.

ticles through a slit (1 cm wide, 76 cm high) that is directed into the wind by a wind vane; the vane pivots on a support in the collector, the top of which is at ground level. The NCAR-modified Bagnold catcher collects particles at six height intervals, the uppermost one from 61 to 76 cm. The collection efficiency at all height intervals has been tested in the Big Spring soil erosion wind tunnel. The Bagnold catcher is a relatively high-volume sampler, compared with the filter collector, and samples are collected for longer time periods so that enough material is collected for size fraction separation by sieving. The sieving was carried out using a sonic sifter system[2] on material collected in the uppermost height interval of the Bagnold catcher. The sifter system uses high-precision electro-formed sieves to separate the collected dust into the size fractions $r<5$ μm, $5<r<10$ μm, $10<r<30$ μm, $30<r<75$ μm, and $75<r<125$ μm; for particles with $125<r<250$ μm, the fractions were separated with sieves of lower precision. The mass distributions obtained by sieving were converted to number distributions by assuming that all of the particles in a particular interval had radii equal to the geometric mean radius of the interval, converting this to an average particle mass, and dividing into the total mass in that size range.

The measured size distribution for the uppermost stage of the Bagnold catcher was corrected for the difference in height between the uppermost stage and 2 m (the height of visibility observations), using the diffusion-sedimentation equilibrium relationship discussed in Gillette and Goodwin (1974). This relationship was found to represent very well the variation in dust concentration with height for wind erosion incidences. In general, the net effect of the height correction is a reduction in the number of all of the particles, with the number of the largest particles reduced the most. The height-adjusted Bagnold size distributions showed that particles with $r>75$ μm contributed very little to the total mass concentration in the air, even for those conditions of severely reduced visibility which we observed.

Since the Bagnold catcher becomes relatively inefficient as a particle collector for particles with $r<10$ μm, the range $10<r<30$ μm was the lowest size range used for the Bagnold data. The size distribution obtained with the Bagnold data was added to the distribution obtained by filtration and microscopic counting for particles with $r<9.89$ μm to obtain an accurate size distribution over the complete size range. In addition to the complete size distribution, we have also used the distribution obtained by filtration only, with both inclusion and exclusion of data for $r>10$ μm to determine the effect of a simpler particle-sizing analysis on calculated visibilities. A typical measured size distribution determined by our automated image-scanning system and the Bagnold sampler data for $r<0.62$ μm is shown as the solid line in Fig. 4. In this bimodal distribution, the mode with mean radius >10 μm is characteristic of the distribution of particles in the soil, while the mode with mean radius <10 μm is due to soil aggregates that have been dispersed by sandblasting. The dashed line in this figure represents a typical size distribution for particles with $r<1.0$ μm determined by using the scanning electron microscope.

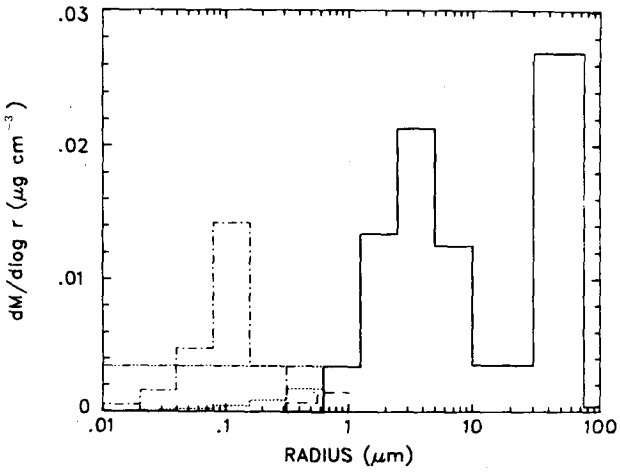

FIG. 4. Typical size distributions for aerosols 2 m above the surface, measured by the automated particle sizing and Bagnold sieving techniques (——), and by scanning electron microscope techniques (– – –) and three artificial distributions, MOD1 (–·–·–), MOD2 (–··–) and MOD3 (····) assumed for the smaller particles. The artificial distributions, described in the text, are chosen in each case to agree with the observed distribution in the smallest range measured.

5. Method of comparison of observed and calculated visibilities

The method to be discussed in this section directly compares observed and calculated visibilities; it uses a least-squares fitting routine and compares observed data to calculated data by means of a χ^2 analysis in order to determine whether the calculated visibilities are in quantitative agreement with the observed visibilities. Such a comparison was chosen rather than the more common method of calculating a correlation coefficient because a correlation coefficient is useful for determining only whether two variables are related but not the exact form of the relation. The least-squares analysis does provide the quantitative information needed for our comparisons.

With perfect agreement between calculated and observed visibilities, we would have $V_{calc}=V_{obs}$, with calculated visibilities equalling the observed visibilities for each data point. The agreement is not perfect, however, and, for analysis the observed visibility is considered to be a function of the calculated visibility with $V_{obs}=f(V_{calc})$. Because the data vary over nearly three orders of magnitude, and because the uncertainty

[2] ATM Corporation, Milwaukee, Wisc.

in the data is approximately a constant percentage of the observed visibility, an appropriate fit to the data is a relation between the logarithms of V_{obs} and V_{calc}. Thus, a linear least-squares fitting routine may be applied to the expression

$$\ln V_{obs} = \ln A + B \ln V_{calc}. \quad (8)$$

(If $V_{obs} = V_{calc}$, then $\ln A = 0$ and $B = 1$.)

The method of least squares (or maximum probability) is based on the assumption that the best-fit parameters maximize the probability that the observed data points are measurements of data described with these parameters. This is equivalent to minimizing the quantity χ^2, which is defined by Bevington (1969) as

$$\chi^2 = \sum \left(\frac{\Delta y_i}{\sigma_i}\right)^2 = \sum \left[\frac{1}{\sigma_i^2}(y_i - a - bx_i)^2\right], \quad (9)$$

where Δy_i is the deviation of each point from the fitted line; y_i and x_i are data points; a and b are fitting parameters for a regression line of the form $\hat{y}_i = a + bx_i$; $\hat{y}_i$ is the calculated value of y at x_i; and σ_i is the standard deviation associated with each point. When applied to the logarithms of the dependent and independent variables, this method does not require a knowledge of the standard deviation of the absolute value of each point, but only of the relative magnitudes of the uncertainties. For Eq. (8), the formula becomes

$$\chi^2 = \sum \frac{1}{\sigma_i^2}(\ln V_{obs,i} - \ln A - B \ln V_{calc,i})^2. \quad (10)$$

Since there is an approximately equal percentage of uncertainty in each point in our data set, the σ_i values, which are standard deviations of the logarithms of the points in Eq. (10), are assumed to be equal.

In the fitting procedures, χ^2 is minimized by differentiating χ^2 with respect to $\ln A$ and with respect to B. For computational purposes, we estimate the total uncertainty to be approximately a factor of 2, leading to an estimated constant value of $\ln 2$ for the standard deviation. A new parameter, the "reduced chi-square," χ_ν^2, may be determined by dividing χ^2 by the number of degrees of freedom in the data; that is, the number N_0 of data points minus the number of parameters that have been fitted to these data points. If, for example, two parameters have been fitted to a data set, then

$$\chi_\nu^2 = \frac{1}{N_0 - 2}\chi^2. \quad (11)$$

When parameters are not fitted, as is the case when data are compared with an expected function, then

$$\chi_\nu^2 = \frac{1}{N_0}\chi^2. \quad (12)$$

The importance of χ_ν^2 is that it characterizes how well the data are fitted by a function with particular parameters. A good fit is indicated by a value of $\chi_\nu^2 \lesssim 1$. Values of χ_ν^2 significantly greater than 1 indicate a poor fit, and the greater the value of the reduced chi-square, the worse the fit. A discussion of the reduced chi-square parameter is found in Bevington (1969).

TABLE 1. Coefficients for least-squares fit and corresponding values of χ_ν^2 for all data sets:

$\ln V_{obs} = \ln A + B \ln V_{calc}$.

Distribution	A	B	χ_ν^2
Expected values	1.00	1.00	
REAL	0.92	0.96	0.88
MOD1	3.67	0.94	7.84
MOD2	2.75	0.98	5.35
MOD3	1.43	0.98	1.53
MOD4	0.38	0.90	5.52
FILTER1	0.85	0.95	0.94
FILTER2	0.87	0.92	0.92

An alternate approach to the problem of comparing the observed and calculated data leads to a refined estimate of the standard deviation of the points in the data set. Here, the calculated standard deviation is obtained by a standard curve-fitting routine that returns the value for σ_i that leads to the reduced chi-square value $\chi_\nu^2 \equiv 1$. The results of such calculations for our measured size distribution as well as for several modified data sets are shown in Table 1 and in Figs. 5–11.

6. Comparison of observed and calculated visibilities for REAL data set

Observed visibilities have been matched with 13-point visibilities calculated on the basis of measured size distributions and the optical properties for airborne soil particles measured by Grams *et al.* (1974) to form the basic data set (which we have designated as REAL). A plot of the observed visibilities versus the calculated visibilities for this REAL data set is shown in Fig. 5; the best-fit line and the calculated standard deviation are also shown. It is readily apparent from the figure that there is agreement with the expected $V_{calc} = V_{obs}$ line, with the expected line well within the calculated standard deviation. The computation for the reduced chi-square relative to the expected line, based on the calculated standard deviations, yields a value for χ_ν^2 of 0.88, also indicating good agreement.

7. Effects of varying size distribution and optical properties

Artificial distributions were designed to investigate possible uncertainties in our particle-sizing techniques. The first, second and third artificial distributions (MOD1, MOD2 and MOD3), shown in Fig. 4, were

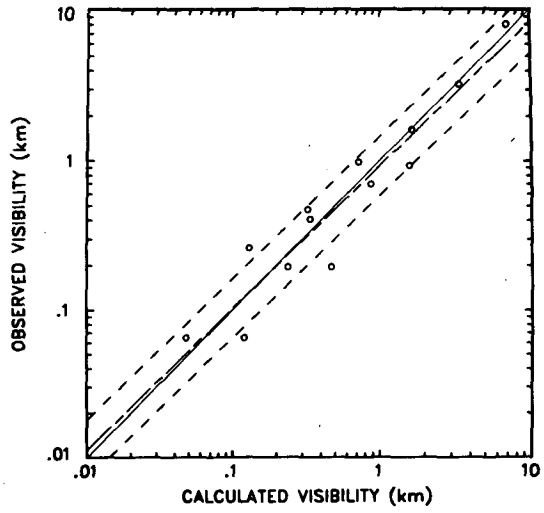

FIG. 5. Observed vs calculated visibilities for the REAL data set. Solid line is the expected $V_{calc}=V_{obs}$ line; the line with long and short dashes represents the best-fit line to the data, while the two uniformly dashed lines on either side of the best-fit line indicate the standard deviation calculated for the data.

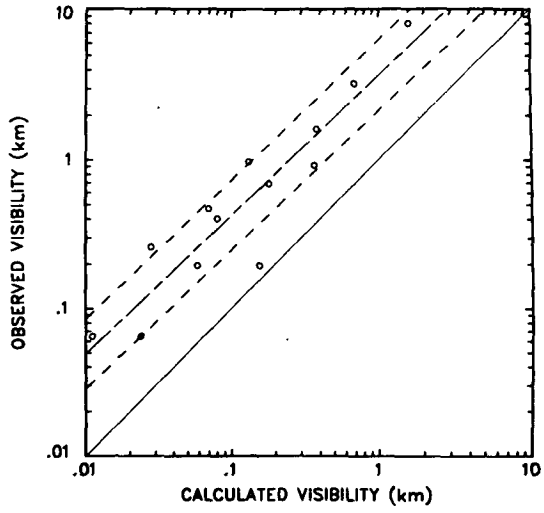

FIG. 6. As in Fig. 5 except for the MOD1 data set.

designed to investigate the effect of relatively large numbers of smaller particles on our calculated point visibilities, an investigation that seemed warranted because we had not analyzed particles with $r<0.62$ μm for all samples. In each case, the size distribution function for the smaller particles present was chosen to be continuous with the observed size distribution in the radius interval from 0.62 to 1.24 μm.

MOD1 is a distribution similar to that measured by Sverdrup *et al.* (1975), in which concentrations of particles with $r<0.62$ μm are introduced to give a bimodal mass-size distribution for particles with $r<10$ μm; there is an approximately equal mass in each mode, and the small-particle mode is centered in the size range $0.08<r<0.16$ μm. This distribution includes very large numbers of particles in the smaller size ranges, with a resulting large contribution to the total extinction. It would be highly unlikely to observe such a distribution, since the small-particle mode is characteristic of combustion and photochemical aerosols which are not significant under our experimental conditions (i.e., a rural area characterized by soil erosion). Thus, it is not surprising that this distribution gives poor agreement with the expected line which had shown good agreement between the observed visibilities and those calculated from the REAL size distribution. Visibilities calculated for this distribution and best-fit lines are shown in Fig. 6; the reduced chi-square calculated relative to the expected line is 7.84, indicating an extremely poor fit.

A possibly more realistic assumption is that small particles are present and that they are distributed according to a power-law distribution function in which

$$dN/d\log r \propto r^{-\nu}. \qquad (13)$$

MOD2 was chosen with $\nu=3$, for which $dV/d\log r$ is a constant for the smaller particles. This is the function commonly referred to as the "Junge distribution" for atmospheric aerosols (Junge, 1963). Visibilities and best-fit lines calculated with this distribution are shown in Fig. 7; the line $V_{obs}=V_{calc}$ still lies outside the calculated standard deviations, and χ_ν^2 relative to the expected line is 5.35. Any such assumed distribution with an exponent larger than 3 gives even poorer agreement. Calculated visibilities for a power-law distribution with $\nu=2$ (MOD3) are shown in Fig. 8. The calculated value of χ_ν^2 is 1.53, significantly larger than the value of 0.88 obtained with REAL, although the expected line lies within one standard deviation of the best-fit line. Consideration of these and other distributions led to the conclusion that if small particles were present, they were present in numbers no larger than

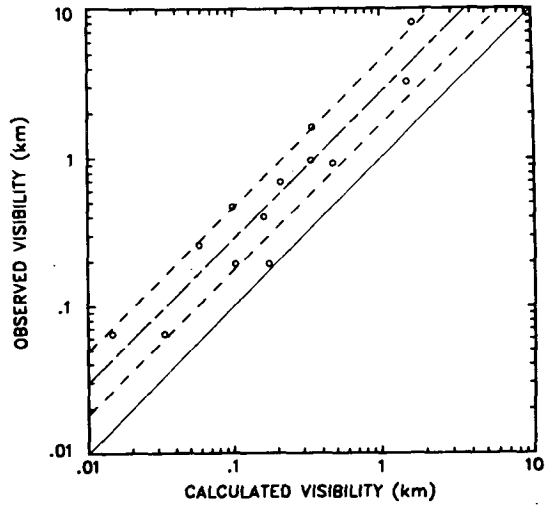

FIG. 7. As in Fig. 5 except for the MOD2 data set.

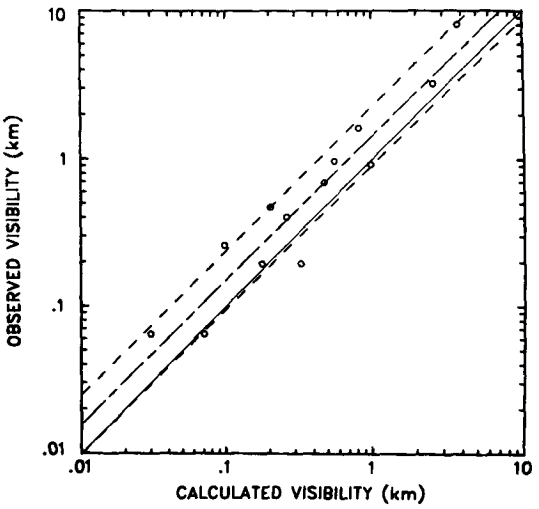

FIG. 8. As in Fig. 5 except for the MOD3 data set.

that given by a Junge distribution with $\nu=2$, for which the total mass differs from the observed mass by less than 5%.

An additional size distribution (MOD4) investigated was one in which the total mass measured was assumed to be correct, but in which all of the mass for particles with $r<10$ μm was concentrated in the size range from 4.96 to 9.89 μm. The rationale for this test is the data presented by Chepil (1957), who measured particle size distributions for airborne dust and found virtually no particles with $r<10$ μm. Our measurements of smaller particles might be explained by postulating the breakup of aggregates on impaction with the filter. Our analysis of the calculated visibility data based on the MOD4 distribution, shown in Fig. 9, results in a χ_ν^2 of 5.52, leading to the conclusion that such an assumption is not correct, although the possibility of some breakage cannot be completely discounted.

We have also investigated the effect of varying the imaginary index of refraction of the particles from $n_{\mathrm{Im}}=0$ to $n_{\mathrm{Im}}=0.05$. For the cases calculated, there were essentially no changes in the fitted lines and uncertainties; the maximum χ_ν^2 calculated was equal to 0.89, compared with 0.88 for the REAL case. Similar checks using the scattering coefficient Q_{SCA} rather than the extinction coefficient Q_{EXT} were made for three values of the imaginary index of refraction, $n_{\mathrm{Im}}=0$, 0.005 and 0.01. These calculations showed best-fit lines with increasing deviation from the best-fit line as the imaginary index is increased. For the REAL data with $n_{\mathrm{Im}}=0.01$, $\chi_\nu^2=1.78$, which is significantly greater than 1. Thus, the absorptive properties of the aerosol cannot be neglected by applying Q_{SCA} data to observed particle size distributions in order to calculate visibilities, and a measurement of total scattering coefficient is not equivalent to measurement either of the total extinction or of the visibility when $n_{\mathrm{Im}}>0$.

8. Results of simplified size-determination procedures

We have also calculated the visibility on the basis of filter size determinations only, both excluding and including the range from 9.89 to 19.73 μm. The results of these distributions, FILTER1 and FILTER2, are shown in Figs. 10 and 11. FILTER1 (using only the lower size range) results in best-fit parameters that are close to the REAL case (Table 1), with $\chi_\nu^2=0.94$. The agreement is slightly improved by including the range from 9.89 to 19.73 (designated FILTER2) which results in the calculated value $\chi_\nu^2=0.92$. This agreement implies that the size distributions that include the small particle mode only are adequate as predictors of ob-

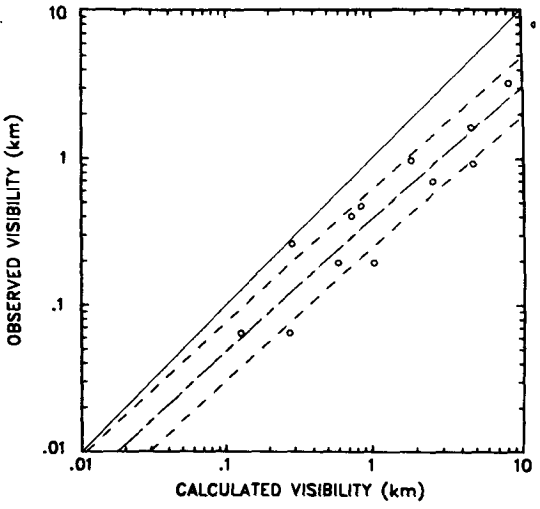

FIG. 9. As in Fig. 5 except for the MOD4 data set.

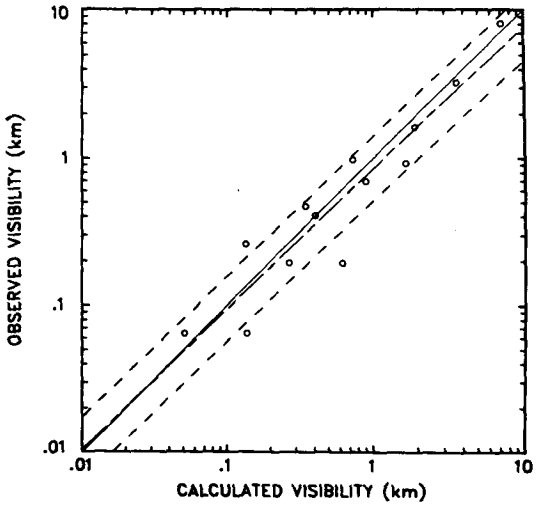

FIG. 10. As in Fig. 5 except for the FILTER1 data set.

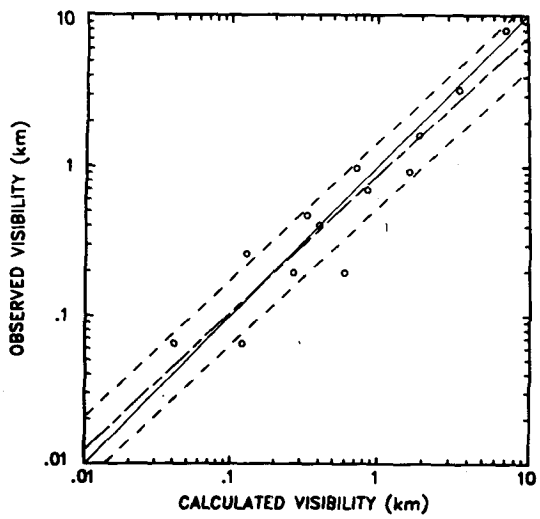

FIG. 11. As in Fig. 5 except for the FILTER2 data set.

served visibility. Since a significant and highly variable proportion of the total particulate mass concentration of material in the atmosphere may be due to particles in the large particle mode, a further implication is that a single relationship between mass concentration and visibility is not generally applicable when the reduction in the visibility is caused by dust due to soil erosion. Furthermore, since the scattering is not equivalent to the extinction when $n_{\mathrm{Im}} \neq 0$, we also have the implication that measurements of total scattering (e.g., by a device such as an integrating nephelometer) cannot be definitively related to either the total extinction or the mass concentration of windblown dust unless both size distribution and optical properties are known.

9. Conclusions

We have made simultaneous visibility observations and particle size determinations from which point visibilities were calculated. These calculated and observed visibilities have been compared, with good agreement. Similar checks with modified size distributions showed that any significant changes in our measured size distributions produced major discrepancies between the observed and calculated visibilities. It was found that variations in the imaginary index of refraction had almost no effect on the visibilities calculated using Mie formulas for extinction; calculations involving total scattering only gave erroneous results for absorbing particles in the sizes observed. It was also found that under our experimental conditions the contributions to the total extinction from the particles with $r > 20$ μm could be neglected and that the size distributions obtained from our filtration procedures only were sufficient to calculate point visibilities that agree with the observed visibilities; the optically important particles were those in the size range $0.62\lambda < 20$ μm. In general, our results show that simple visibility observations can provide useful checks on the size distributions measured for atmospheric particulate matter, and that such checks, applied to our measured size distributions, confirm the accuracy of our sizing techniques for the aerosols measured. Although our data are only for conditions in which the visibility reduction is due to windblown dust, the fact that significant changes in the measured size distributions produced discrepancies between observed and calculated visibilities implies that visibility measurements should be useful as size distribution checks under a variety of experimental conditions, for both rural and urban aerosol studies.

REFERENCES

Bevington, P. R., 1969: *Data Reduction and Error Analysis for the Physical Sciences*. McGraw-Hill, 438 pp.

Blifford, I. H., and D. A. Gillette, 1973: An automated particle analysis system. *Microscope*, **21**, 212–230.

Chepil, W. S., 1957: Sedimentary characteristics of dust storms: III. Composition of suspended dust. *Amer. J. Sci.*, **255**, 206–213.

——, and N. P. Woodruff, 1957: Sedimentary characteristics of dust storms: II. Visibility and dust concentration. *Amer. J. Sci.*, **255**, 104–114.

Deirmendjian, D., 1969: *Electromagnetic Scattering on Spherical Polydispersions*. Elsevier, 290 pp.

Ensor, D. S., R. J. Charlson, N. C. Ahlquist, K. T. Whitby, R. B. Husar and B. Y. H. Liu, 1972: Multiwavelength nephelometer measurements. *Aerosols and Atmospheric Chemistry*, G. M. Hidy, Ed., Academic Press, 348 pp.

Gillette, D. A., I. H. Blifford, Jr., and C. R. Fenster, 1972: Measurements of aerosol size distributions and vertical fluxes on land subject to wind erosion. *J. Appl. Meteor.*, **11**, 977–987.

——, and P. A. Goodwin, 1974: On the microscale transport of sand sized wind erosion soil aggregates. *J. Geophys. Res.*, **79**, 4080–4084.

Grams, G. W., I. H. Blifford, Jr., D. A. Gillette and P. B. Russell, 1974: Complex index of refraction of airborne soil particles. *J. Appl. Meteor.*, **13**, 459–471.

Huschke, R. E., Ed., 1959: *Glossary of Meteorology*. Amer. Meteor. Soc., 638 pp.

Johnson, J. C., 1954: *Physical Meteorology*. The MIT Press, 68–104.

Junge, C. E., 1963: *Air Chemistry and Radioactivity*. Academic Press.

Kerker, M. E., 1969: *The Scattering of Light and Other Electromagnetic Radiation*. Academic Press, 666 pp.

Koschmieder, H., 1924: Theorie der horizontalen Sichtweite. *Beitr. Phys. Atmos.*, **12**, 33–53.

Spurny, K. R., J. P. Lodge, Jr., E. R. Frank and D. C. Sheesley, 1969: Aerosol filtration by means of nuclepore filters. Structural and filtration properties. *Environ. Sci. Tech.*, **3**, 453–464.

Sverdrup, G. M., K. T. Whitby and W. E. Clark, 1975: Characterization of California aerosols II. Aerosol size distribution measurements in the Mojave Desert. *Atmos. Environ.*, **9**, 483–494.

U. S. Department of Commerce, U. S. Department of Defense, U. S. Department of Transportation, 1970: Federal Meteorological Handbook No. 1, *Surface Observations*, 7th ed., Washington, D. C., U. S. Govt. Printing Office.

van de Hulst, H. C., 1957: *Light Scattering by Small Particles*. Wiley, 470 pp.

Zuev, V. E., B. B. Koshlev, S. D. Trorogov and S. S. Khemleutsov, 1965: Attenuation of visible and infrared radiation by artificial water fogs. *Izv. Atmos. Oceanic Phys.*, **1**, 298–301.